4.1 Introduction

In Chapter 3, many interesting properties has been shown by Cu doped Bi_2Te_3 such as tuning of carrier from n type to p type, SdH oscillation in magneto-resistance experiment and ferromagnetism. It was also observed that ferromagnetism was increasing with the increase in Cu concentration, hence doping of Cu at higher concentration may be the matter of interest. Moreover, materials with large magnetoresistance (MR) are of great interest from the application point of view as well as for fundamental research. According to Abrikosov's theory [35], a quantum linear magneto resistance, is expected in the materials having zero band gap with linear energy spectrum whereas Parish and Littlewood (PL) have proposed a classical model for the explanation of MR in the inhomogeneous system having strong disorder such as nonmagnetic graphene, $Ag_{2\pm\delta}Se$ and $Ag_{2\pm\delta}Te$, InSb system [56-58] which was based on two-dimensional random register network. Materials with linear MR might be used in magneto electronic applications. Recently, a giant and linear MR in TIs has been reported [59-61]. Zhang et al. showed that on ultra thin film of Bi_2Se_3 a surface state gap opened at the Dirac point because of tunneling between the top and bottom surface states [62]. Study of 5% Cu doping (x=0.15) on Te site in Bi_2Te_3 has been reported in this chapter. It is observed from Hall resistivity and thermoelectric data that type of carrier changed from *n* type to *p* type with Cu doping which is same as the previous case mentioned in chapter 3. Also in the doped sample the magnetoresistance was changing from linear to non-linear behavior at low temperature but at higher temperature (>100K) it again becomes linear.

Furthermore, beside the interesting features in TIs, breaking of time reversal symmetry on the surface may open a new way for applications. Therefore, magnetically doped TIs have recently been attracted great interest for their promising applications in the emerging field of

spintronics and many other novel phenomena previously discussed. Jo et al. [31] reported study on Fe doped Bi_2Te_3 in paramagnetic state, Kulbachinskii [63] have observed that Bi_2Te_3 becomes ferromagnetic by Fe doping with c axis as the easy magnetization axis and Curie temperature (T_C) below 12K. Watson et al. [64] found that Mn doped Bi_2Te_3 are soft ferromagnets with small coercive field and $T_C \approx 9.4K$ whereas Hor et al. [30] demonstrated that very weak ferromagnetic exchange energy may responsible for the small coercivity and weak ferromagnetism in Mn doped Bi_2Te_3 which showed second order ferromagnetic transition with a T_C of approximately 12K, but ferromagnetic ordering at room temperature is required for the spin based applications. In this chapter, we have investigated the structural, magneto-transport and magnetic properties of Cu doped Bi_2Te_3 which shows tuning of carrier type from *n* to *p* type, high carrier concentration and mobility, large magnetoresistance and room temperature ferromagnetism which are important for quantum computing, spintronic devices, multifunctional electromagnetic application and disc reading heads.

4.2 Results & Discussion

4.2.1 X-Ray analysis

Single crystals of $Bi_2Cu_xTe_{3-x}$ (x=0, 0.15) with the cleaved surface along the basal planes were characterized using X-ray diffraction (XRD) method collected at room temperature. X-ray diffracted beam directions showed only the (00L) with space group D_{3d}^5 (R-3m). The XRD pattern of $Bi_2Cu_xTe_{3-x}$ (x=0, 0.15) samples are shown in Fig. 4.1. All the peaks of the as obtained XRD patterns have been indexed using the standard JCPDS file (JCPDS#15-0863). Moreover, the peak positions are consistent with those of already reported data [37]. All peaks positions of pure and Cu doped Bi_2Te_3 well matched to the standard Bragg's positions of Rhombohedral structure of Bi_2Te_3. It is obvious from the XRD

patterns that the Cu doping does not lead to the presence of any extra peaks or absence of any peaks of the rhombohedral structure of pure Bi_2Te_3 which indicates that the structure of the Cu doped Bi_2Te_3 retains the rhombohedral crystal structure belonging to the space group D_{3d}^5(R-3m). Laue pattern of $Bi_2Cu_{0.15}Te_{2.85}$ sample is shown in inset of Fig.4.1.The Full Width Half Maxima (FWHM) of the (003) peak was 0.115^0 and 0.125^0 whereas for (006) peak it was 0.131^0 and 0.137^0 for pure and Cu doped samples respectively, which are very small indicating that as prepared samples have excellent single crystallinity in long range. Around $2\theta=54^0$ and 64^0, a small splitting due to the CuK_β radiation is observed. An additional peak around $2\theta=27.6^0$ and 40^0 for both the samples is observed which might

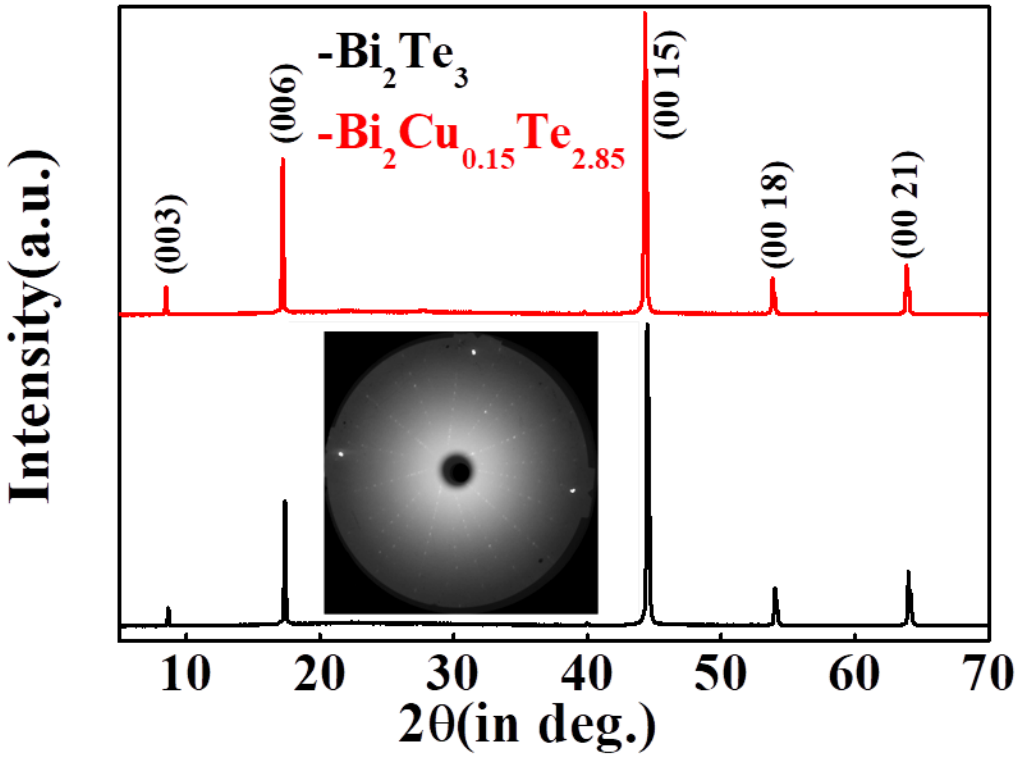

Fig.4.1 Room temperature X-ray diffraction patterns of Bi_2Te_3 and $Bi_2Cu_{0.15}Te_{2.85}$, Inset: Laue pattern of $Bi_2Cu_{0.15}Te_{2.85}$.

be due to the slight misalignment or slight tilt angle of the crystallinity of as cleaved single crystals. A small shift of ~$0.15^0 \pm 0.02^0$ in every peak position towards lower angle in 2θ value is seen in the doped sample. As a matter of fact, according to Bragg's law, interplaner spacing (d) increases with Cu doping. The obtained lattice parameters for pure Bi_2Te_3 sample was $a=b=4.55$Å and $c=30.52$ Å and the cell volume V was 547.72 $Å^3$ whereas the lattice parameters for Cu doped sample was $a=b=4.46$Å and $c=30.61$Å and the obtained V was 528.27 $Å^3$, which were consistent with the reported values [31]. Shift in Bragg's angle and the change in the lattice parameters also support the doping of Cu at Te site. The values of *a*, *b* parameters and the cell volume of doped sample are lower than those values for undoped sample which is attributed to the smaller ionic radius of Cu than that of Te. The slightly elongated *c* parameter in doped sample do not however compensate the decreased a and b parameters in maintaining same lattice volume, leading to smaller cell volume.

4.2.2 Angle Integrated Photo electron Spectroscopy (AIPES) study

The valence band spectra were collected for Bi_2Te_3 and $Bi_2Cu_{0.15}Te_{2.85}$ for a range of photon energies from 16 eV to 27 eV in the angle integrated mode of photoelectron detection (not shown). Such a range of photon energy was chosen for these compounds based on previous experience [65]. Based on the inelastic mean free path (IMFP) of the photoelectrons [66], it is concluded that the surface probing depth for $h\nu=16$ eV becomes almost twice as large as that for $h\nu=27$ eV. Hence we demonstrate in Fig.4.2 the evolution of the electronic structure across bulk and surface for both the compounds, by comparing the density of states (DOS) obtained at the two extreme photon energies. The DOS was obtained by the well known procedures of division of the valence band spectrum by the Fermi distribution function and the symmetrization procedure [67] (shown in the inset of Fig. 4.2(a) and

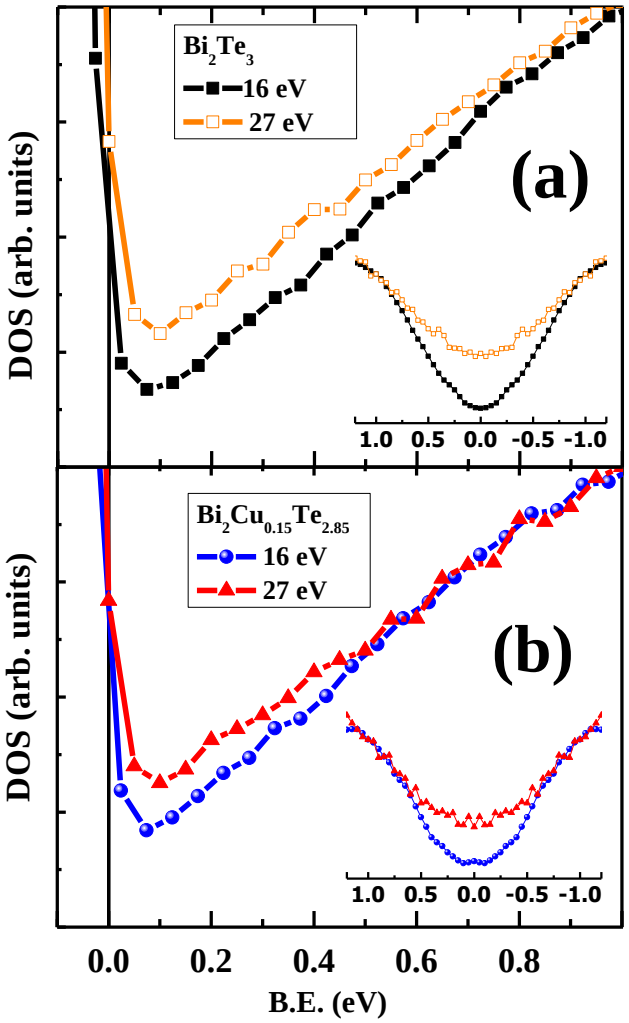

Figs.4.2 (a, b) Valence Band studies of Bi_2Te_3 and $Bi_2Cu_{0.15}Te_{2.85}$ by Angle Integrated Photoemission Spectroscopy.

Fig.4.2 (b)). Both the procedures agree with each other in that both show that the surface is more metallic than the bulk which is expected from a topological insulator. This holds true for both the compounds studied. Thus the photoemission results allow us to characterize the surface metallicity of the topological insulator surface. Therefore, the photoemission results together with bulk measurements indicate a reliable topological insulating behavior of Bi_2Te_3 and $Bi_2Cu_{0.15}Te_{2.85}$ single crystals.

4.2.3 Transport Property analysis

In order to see the electrical transport behavior of the materials, temperature variation of resistivity under zero magnetic fields for pure and Cu doped Bi_2Te_3 samples were carried out [Fig. 4.3 (a)]. It is observed that the resistivity increases with temperature for both pure and doped Bi_2Te_3 samples indicating typical metallic behavior. Fig. 4.3(b) shows the variation of Seebeck coefficient with temperature for both the Bi_2Te_3 and $Bi_2Cu_{0.15}Te_{2.85}$ samples in the temperature range of 10K-300K. Seebeck coefficient for pure Bi_2Te_3 sample shows negative slope whereas $Bi_2Cu_{0.15}Te_{2.85}$ sample shows positive slope in the whole range of temperature indicating a change-over in carrier type from *n* to *p* with Cu doping in Bi_2Te_3, Moreover, the maximum absolute value of Seebeck coefficient in case of Bi_2Te_3 is 142.8μv/K whereas in doped sample it is around 159.8μV/K. The values are consistent with those reported by Cao et.al. [68]. Recently Seebeck coefficient of Bi_2Te_3/Cu composite has been reported. It is observed as the Cu content increases the value of the Seebeck coefficient increases but it remains negative [69]. In the present investigation doping of Cu is not only tuning the carrier type but also increasing absolute value of Seebeck coefficient. It has been reported [31] that if bulk single crystal Bi_2Te_3 is prepared using stoichiometric melting, Tellurium rich composition generates *n* type charge carriers because of Te_{Bi} antisite defects i.e. some of the Te atoms occupy the Bi vacancies. As a consequence, *n* type charge carriers are generated such that Fermi level touches the bulk conduction band. In the same way, when an excess Bi is incorporated in Te sites, then Bi_{Te} antisite defects become dominant and Bi atoms occupy the Te sites. Bi rich composition thus becomes *p* type and Fermi level

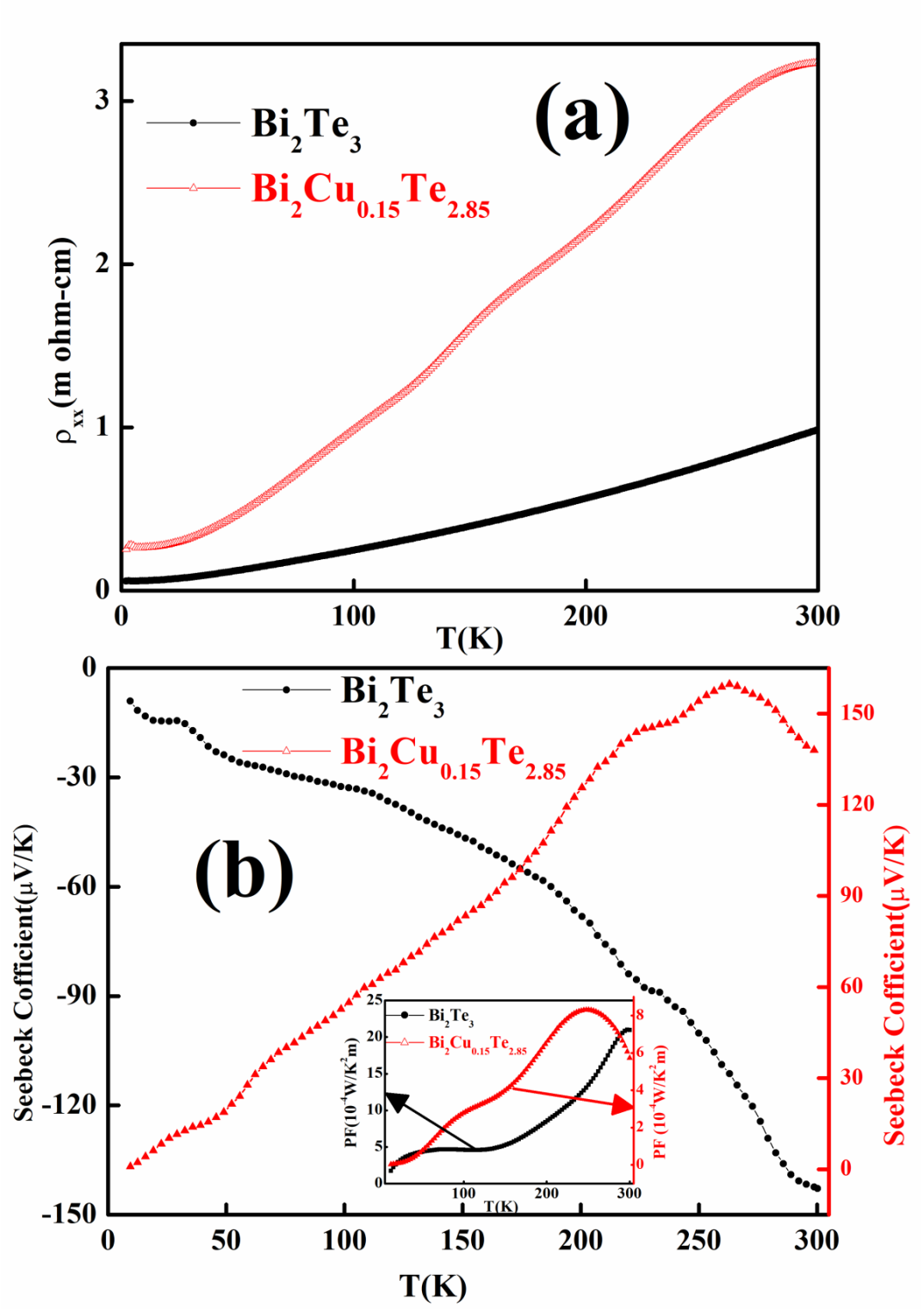

Figs.4.3 (a) Temperature dependence of electrical resistivity for Bi_2Te_3 and $Bi_2Cu_{0.15}Te_{2.85}$ and (b) Variation of Seebeck coefficient as a function of temperature. Inset represents the power factor (PF) of the Bi_2Te_3 and $Bi_2Cu_{0.15}Te_{2.85}$.

touches the valence band. Hence, doping of Cu increases the Bi_{Te} antisite defects and the consequent *p* type carriers result and Fermi level moves from the conduction band to bulk valence band. This gives rise to the suppression in carrier mobility and increment in electrical resistivity.

To determine the efficiency of thermoelectric power we have calculated the power factor [shown in the inset of Fig. 4.3(b)] of doped and undoped samples using the formula

$$\text{Power factor (PF)} = S^2/\rho$$

Where ρ is the electrical resistivity and S is the Seebeck coefficient. It has already been shown that with increase of the temperature electrical resistivity increases in both pure and doped samples but the increase in Seebeck coefficient (S) is much larger than the increase of electrical resistivity which gives rise to the increase of power factor with increasing temperature.

In order to determine the carrier concentration (*n* or *p*) and mobility (μ) of the pure and Cu doped Bi_2Te_3, we have also carried out the Hall measurement. The carrier concentration has been calculated using the slope of the Hall resistivity. Using the data of carrier concentration and electrical resistivity we determined carrier mobility of the samples. Fig. 4.4(a) shows the variation of Hall resistivity as a function of applied magnetic fields at temperatures 200K and 300K for pure Bi_2Te_3. Slope of the curve is negative which shows that carriers in pure Bi_2Te_3 are *n* type for the entire range of temperature of measurement which is similar to the previous case mentioned in chapter 3, the result is also consistent with the negative Seebeck coefficient of the sample. Calculated carrier concentration (*n*) of the pure Bi_2Te_3 is shown in the inset I of Fig. 4.4(a) which comes in the range of reported value

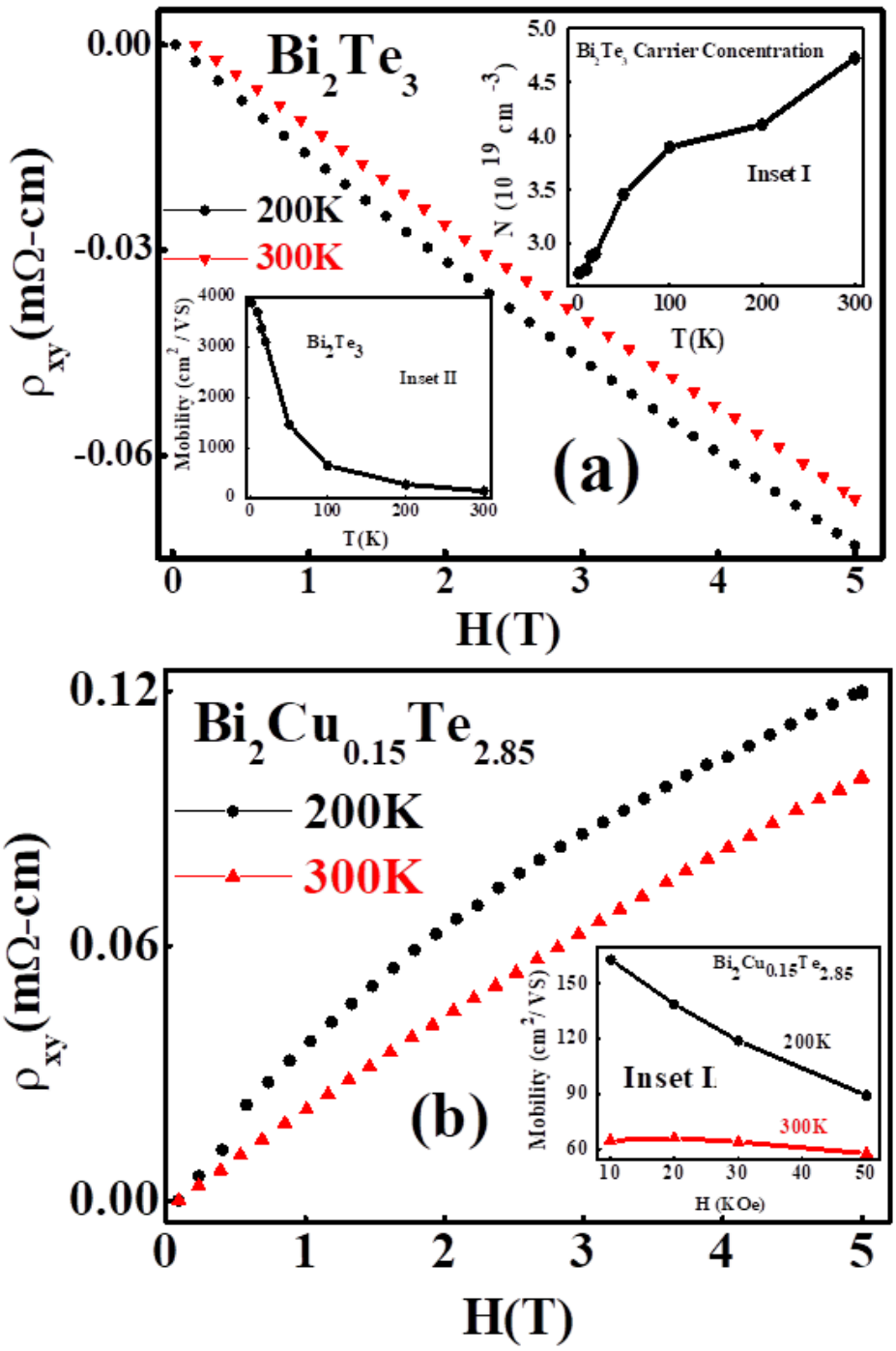

Fig. 4.4 (a) Magnetic field dependence of the Hall resistivity of the Bi_2Te_3 at 200K and 300K, Inset I represents the variation of carrier concentration as a function of temperature whereas Inset II shows the variation of carrier mobility with temperature for Bi_2Te_3 and (b) Magnetic field dependence of the Hall resistivity of the $Bi_2Cu_{0.15}Te_{2.85}$at 200K and 300K, Inset is the variation of carrier mobility as a function of applied magnetic field at 200K and 300K.

given by Zhang et.al. [41].Since topological insulators are insulating in bulk but conducting on surfaces, at high temperature bulk contribution dominates over surface contribution of the sample. As we know topological surface state is a complete quantum phenomenon, existence of quantum mechanical behavior is significant at very low temperature. As a matter of fact, at very low temperature surface state is dominating over bulk state and that is why the carrier concentration is low at low temperature ($T \leq 20K$) whereas it is very high at high temperature. Moreover, the rate of increment of carrier density is also increasing with the increase of temperature; this also confirms that bulk insulating character is dominating over surface metallic character of the sample at higher temperature. We have also determined the mobility (μ) of the carriers from the Hall data. Calculated mobility as function of temperature is shown in the inset II of Fig. 4.4(a). Mobility for pure Bi_2Te_3 sample at the applied field of 2T is 271.48cm^2/Vsec and 131.68cm^2/Vsec at 200K and 300K respectively whereas at Field 5T it is 225.99cm^2/Vsec and 126.71cm^2/Vsec at 200K and 300K respectively. Hence it is clear that as we increase both the temperature and field, mobility decreases. This is as expected because with decreasing temperature, freezing out of phonons takes place and as a consequence, the carrier scattering and thus thermal vibration or the contribution of phonon decreases and high mobility prevails. Similar trend happens with the magnetic field.

Figure 4.4(b) shows the variation of Hall resistivity with the applied magnetic field for $Bi_2Cu_{0.15}Te_{2.85}$ sample at 200K and 300K. The non-linearity is observed at both the temperatures. We tried to fit the data with two-carrier model [70] (not shown), but the obtained parameters are not feasible. Therefore, the observed non-linearity might be the indication of Anomalous Hall Effect (AHE) due to the existence of ferromagnetism in $Bi_2Cu_{0.15}Te_{2.85}$sample. In a magnetic sample the Hall resistivity depends upon applied field as

well as magnetization of the materials and is expressed as $\rho_H=R_0B+R_M M$ where R_0 is the Hall coefficient, B is the applied magnetic field, R_M is the anomalous Hall coefficient and M is the magnetization of the material. At high fields, the ordinary Hall Effect dominates as is seen by the linear dependence of ρ_H whereas at low fields Anomalous Hall effect dominates. The origin of the ferromagnetism in $Bi_2Cu_{0.15}Te_{2.85}$ will be discussed later. The slope of the curve is positive which shows that carriers are *p* type supporting the observation in Seebeck coefficient. The carrier concentration is 2.20×10^{19} per cm^3 and 2.96×10^{19} per cm^3 at 200K and 300K respectively, which is less than the pure sample. Carrier density increases with temperature similar to the undoped sample. The variation of mobility with the applied field is shown in the inset I of fig. 4.4(b). Mobility decreases with increase in field and temperature as is observed in the Bi_2Te_3 and the value is lower in $Bi_2Cu_{0.15}Te_{2.85}$ than that of the undoped sample which has already been discussed above. It is worthwhile to mention that the presence of foreign element i.e. Cu may also produce extra center of scattering and results higher resistivity as is observed in [Fig. 4.3(a)]. Moreover, mobility, calculated from the Hall measurement in pure sample, is higher than that of doped one giving rise to the low resistivity. Therefore, both Hall data and thermo power data corroborate the resistivity data.

Variation of magneto resistance (MR) as a function of applied magnetic field at different temperatures for pure and doped samples is shown in Figs. 4.5(a) and 4.5(b, c, d), respectively. Figure 4.5(a) shows a clear linear and non-saturating MR of Bi_2Te_3. MR of Bi_2Te_3 increases with applied field but decreases with increasing temperature. A linear and non-saturating magnetoresistance could be clearly seen for the entire range of temperature and field of measurement in pure Bi_2Te_3 sample. No SdH oscillation has been observed in x=0.15 sample similar to the sample x=0.03 and 0.09 discussed in previous chapter III, the

absence of oscillation might be the result of the extra scattering centre produced by the Cu in x=0.15 sample. But in x=0.15 sample at low temperature saturation in magnetoresistance (≤100K) is observed. The tendency of saturation in MR is maximum at lowest temperature (2K) of measurement and decreases gradually as we increase temperature up to 100K. We can easily see the linear curve at 110K up to high magnetic field and above this temperature magnetoresistance remains linear [Fig. 4.5 (b, c, d)]. Besides this linear magnetoresistance (LMR) at high field, the cusp like positive MR at low magnetic field is also observed in $Bi_2Cu_{0.15}Te_{2.85}$ sample indicating weak anti-localization (WAL) supporting the existence of surface state, [71-73] with increase of temperature MR becomes linear for intermediate temperature range and again at higher temperature i.e. at 300K it shows quadratic behavior. Similar behavior without any sign of saturation at high temperature in Bi_2Te_3 has been reported by He et al. [50]. At high temperature the low field MR dip broadened as at higher temperature phase coherence length decreases [50] hence WAL decreases with increasing temperature [Fig. 4.5(d)]. Since the origin of WAL effect is the spin momentum locking at the surface state Dirac cone [50, 74] it requires zero-gap Dirac fermions. Therefore, as with increasing temperature magnetic ordering decreases and the gap approaches to zero, so the WAL also decreases. Moreover, the maximum MR increases with Cu doping (from 375% for undoped sample to 1000% for doped sample) which enhances the potentiality for application. Coupling of Cu mediated spin to the applied magnetic field may be a reason for the large MR value in doped sample. Li et al. [75] observed that when thickness of Bi_2Te_3 thin films is greater than 2QL (quintuple layer) then topological surface state (TSS) appears. He et al. [76] reported that in Bi_2Se_3 thin films of thickness <6nm, grown by molecular beam epitaxial method, linear magnetoresistance disappears due to opening of gap in the surface state as

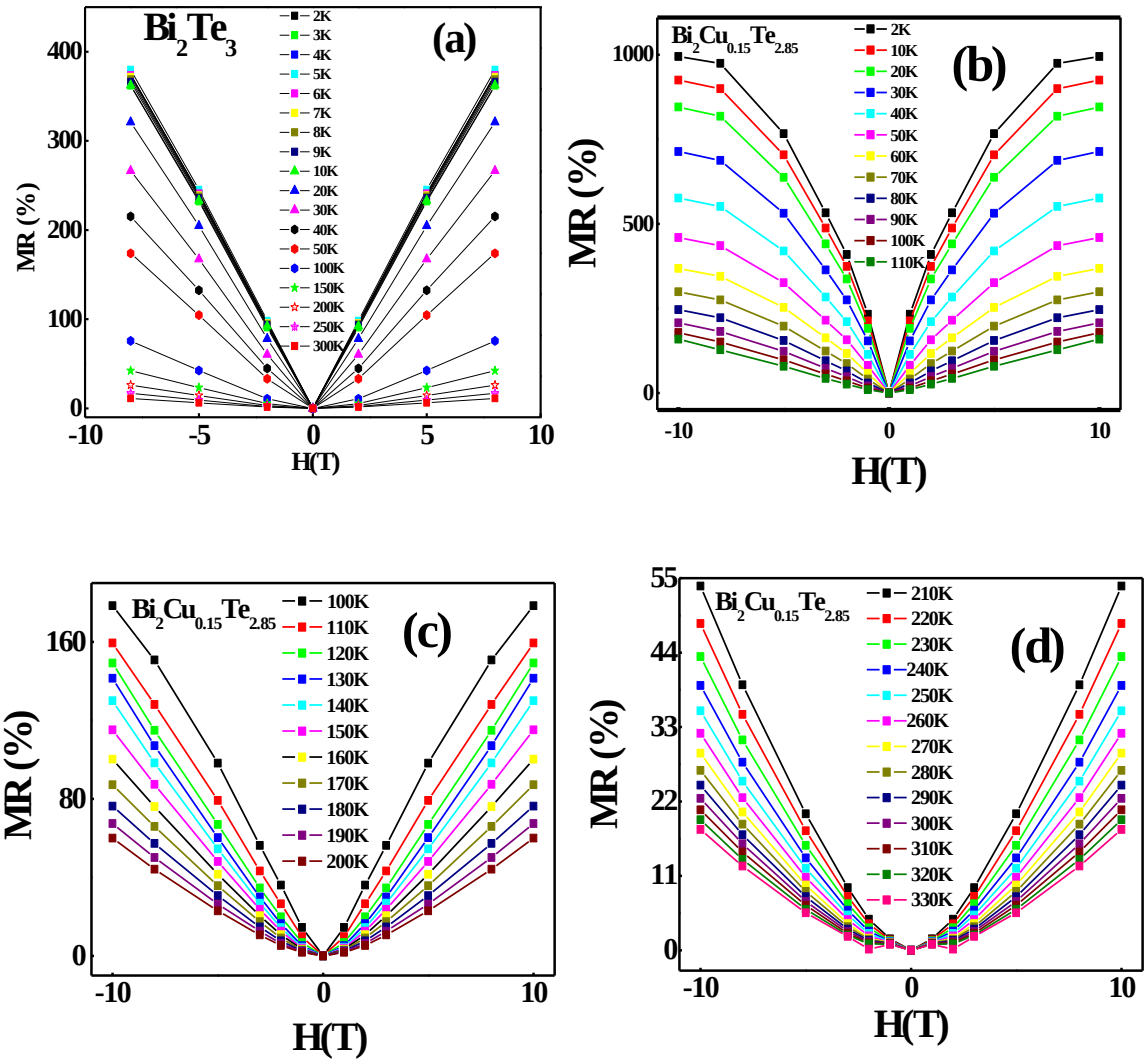

Fig.4.5 (a) Magnetoresistance $=\frac{R(H)-R(0)}{R(0)}X100\%$ as a function of magnetic field for Bi_2Te_3 at different temperatures and (b, c, d) Magnetoresistance $=\frac{R(H)-R(0)}{R(0)}X100\%$ as a function of magnetic field for $Bi_2Cu_{0.15}Te_{2.85}$ at different temperatures.

induced by the interface coupling. In Bi_2Te_3 nanoplates with a thickness of less than 5nm, absence of surface gapless state is observed by Kong et al. [77]. In order to have a bulk band gap for the topological gapless surface state in Bi_2Te_3 plate like samples, thickness should be greater than 14QL. In the present investigation, both the doped and undoped samples are cleaved with few mm thickness, therefore, thickness will be definitely greater than 14QL in the present system as the thickness of 1QL in Bi_2Te_3 is of the order of some nm. As a matter

of fact, thickness cannot be the reason for the absence of LMR in doped sample. Zhang et.al. [62] reported that in ultrathin film of Bi_2Se_3 absence of LMR is observed because of opening of surface state gap at the Dirac point due to the tunneling between top to bottom surface states. Tuning of band gap and changing in Hall resistivity was observed by Lee [78] in silver chalcogenides by using hydrostatic pressure. Xu et al. [79] observed giant positive and linear magnetoresistance in two nonmagnetic narrow band gap semiconductors $Ag_{2+\_\delta}Se$ and $Ag_{2+\_\delta}Te$ having highly disordered stoichiometry. Abrikosov [35] predicted that nonstoichiometry induced disorder can change a narrow band gap semiconductor to a zero band gap with a linear energy spectrum. According to this theory LMR appears in the system having zero band gap with linear energy spectrum similar to the surface state of the topological insulators. The quantum limit requires that applied magnetic field should be so large that only one Landau level participate in the conductivity in such type of gapless state induced by nonstoichiometric disorder. Moreover, According to generic quantum description of galvano-magnetic phenomenon, the longitudinal MR can be represented as $\rho_{xx=}\rho_{yy=\frac{N_i H}{\pi n^2 ec}}$, where ρ_{xx} and ρ_{yy} are the transverse component of magnetoresistance, N_i is the concentration of static scattering centers, H is the applied field, e is the charge of electron, c is the velocity of light and n is the density of electrons. The quantum MR is positive, linear, temperature independent and nonsaturating down to very small fields in such type of systems. According to the above expression resistance is inversely related to the square of the density of electrons (n) which is also not well matched with our experimental data. It is obvious from the Fig. 4.5(a) that MR is independent of temperature up to only 10K in pure Bi_2Te_3 whereas it is completely temperature dependent for the Cu doped sample and MR is decreasing as we increase the temperature [Fig. 4.5(b, c, d)], so on the basis of this fact we can say that

quantum model proposed by Abrikosov [35] is not applicable in our system. Parish and Littlewood (PL) [80] presented a classical model using a random resistor network and argued that strongly inhomogeneous and macroscopically disordered semiconductors will show a non-saturating MR. This model showed that inhomogeneity, disorderness and zero band gap is essential condition for the presence of LMR. According to this classical model, magnitude of the fluctuations in mobility due to disorder is an important factor for the origin of MR, rather than the mobility. It is observed in Fig. 4.5(a, b, c, d) that both MR and mobility decrease with increase of temperature. This behavior is consistent with the PL model [59], hence we expect that the better explanation may be close to classical case.

Moreover, it is observed that magnetic impurities break the TRS and hence disappearance of robust metallicity of the surface in TIs occurs which results in band gap opening [81]. As a matter of fact the LMR is due to the presence of surface state as already reported in bulk Bi_2Te_3 [52]. Moreover, as we have already discussed that there is site and antisite defects i.e. the presence of disorderness in the studied samples, therefore, this disorderness might be a factor at higher temperature for the linearity in MR which is similar to the results obtained by Wang et al. [82] where it has been explained that magnetic field dependent disorder induced by spin fluctuation might be the reason of linear MR.

4.2.4 Study of Magnetic Property

In order to observe the magnetic state we have performed magnetic measurements. Ferromagnetic states have been confirmed by the M(H) curve in doped sample. Fig. 4.6(a) and 4.6(b) show the M(H) curves at temperatures 5K and 50K for both the doped and undoped samples. It is clear from the M(H) curves that doping of Cu is inducing magnetic

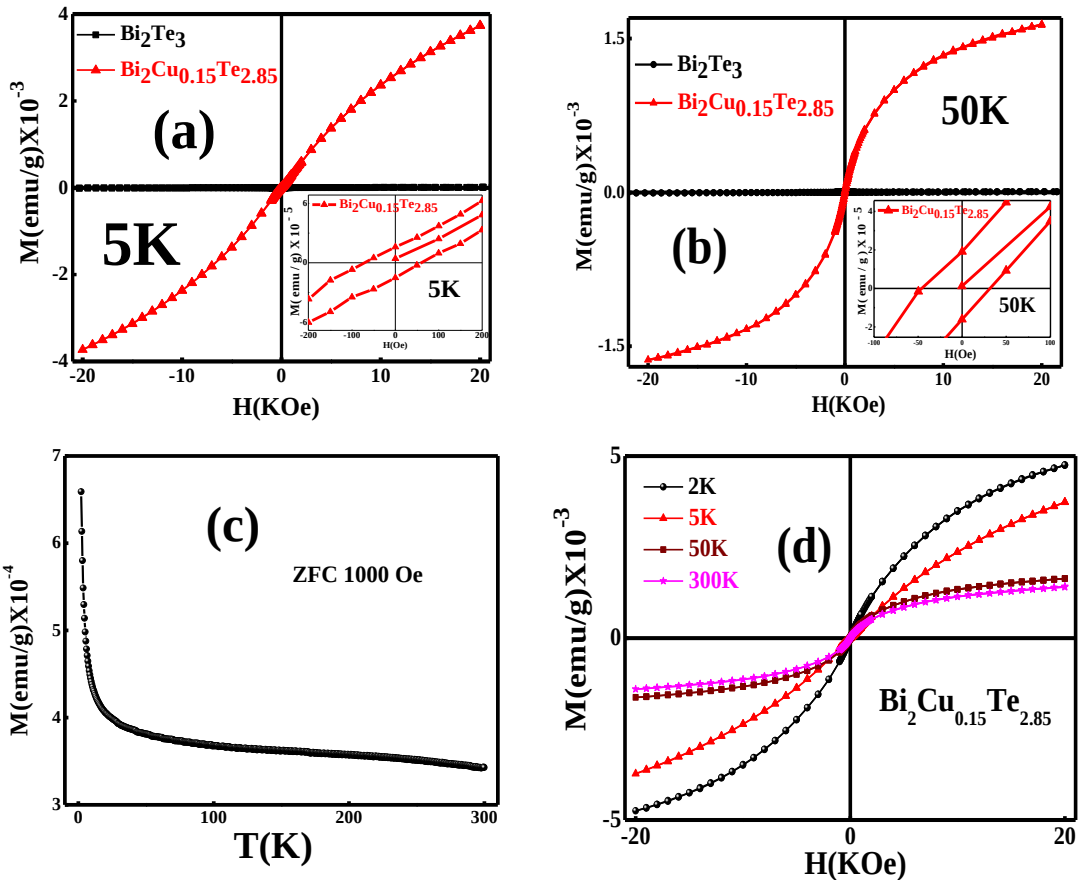

Fig.4.6 (a)-(b) Field dependence of magnetization for Bi_2Te_3 and $Bi_2Cu_{0.15}Te_{2.85}$ samples at 5K and 50K respectively. The inset represents hysteresis in $Bi_2Cu_{0.15}Te_{2.85}$ sample.(c)Temperature dependence of magnetization for $Bi_2Cu_{0.15}Te_{2.85}$ at an applied magnetic field of 1000 Oeshowing ferromagnetic nature.(d) Field dependence of magnetization for $Bi_2Cu_{0.15}Te_{2.85}$ at different temperatures (i.e. 2K, 5K 50K and 300K).

moment. The inset in Figs. 4.6(a) and 4.6(b) at temperatures 5K and 50K clearly show the hysteresis loop indicating that the doping of Cu is tuning the sample from nonmagnetic to ferromagnetic state. The result is also consistent with Hall data of doped sample in which non linearity is observed [Fig. 4.4(b)] which is a clear indication of ferromagnetism. Ferromagnetism has also been reported in magnetic ion (Fe, Cr) doped Bi_2Se_3 [81, 83]. Thus it can be mentioned that the occurrence of ferromagnetism in the present case is due to the non-magnetic Cu doping instead of doping of any ferromagnetic material. In order to provide detail magnetic state of doped sample, we have plotted magnetization (M) vs. temperature (T) and magnetization (M) vs. applied magnetic field (H) for the doped sample in Figs. 4.6(c)

and 4.6(d) respectively. M(T) was measured in the temperature range of $2K \leq T \leq 300K$ at the applied field of 1000 Oe. M(H) measurement of the doped sample was carried out at different constant temperatures (*viz*. at 2K, 5K, 50K and 300K) under the applied field range of -2T to 2T. It is clear from the M(H) curve that sample shows ferromagnetic nature at 2K and the nature of curve remains ferromagnetic even at room temperature.

4.2.5 X-ray photoemission spectroscopy (XPS) analysis

To investigate the origin of ferromagnetism in our doped sample we have collected the detail information about the valence state and chemical bonding of the dopant ions in the parent lattice by X-ray photoemission spectroscopy (XPS) analysis. The spectra of samples were recorded from freshly prepared surfaces at room temperature (RT) where oxygen and carbon contamination were removed via Ar ion sputtering. The binding energies were calibrated with the C1s reference (284.2eV). No other metal ions other than Bi, Te and Cu can be detected in the samples which clearly indicate that as prepared single crystal is pure which is also confirmed by XRD. The experimental data are fitted using XPS peak fit software. Fig. 4.7(a and b) show the core level XPS spectra of Bi4f and Te3d in pure Bi_2Te_3 whereas Figs. 4.7(c, d and e) show the Bi4f, Te3d along with Cu 2p core level spectra of doped sample. Two peaks at 157.2 eV and 162.3 eV in both pure sample and doped samples are observed in high resolution scan of the Bi4f region which correspond to the binding energies of $Bi4f^{7/2}$ and $Bi4f^{5/2}$ spin states, respectively (shown in fig.4.7(a) and fig.4.7(c)), which are consistent with the reported data [63]. Similarly, The fig. 4.7(b) and 4.7(d) reveal two 3d Te spectral peaks at 571.4 and 581.8 for pure and doped samples corresponding to the spin states of Te $3d^{5/2}$ and $3d^{3/2}$ respectively, also well matched with the

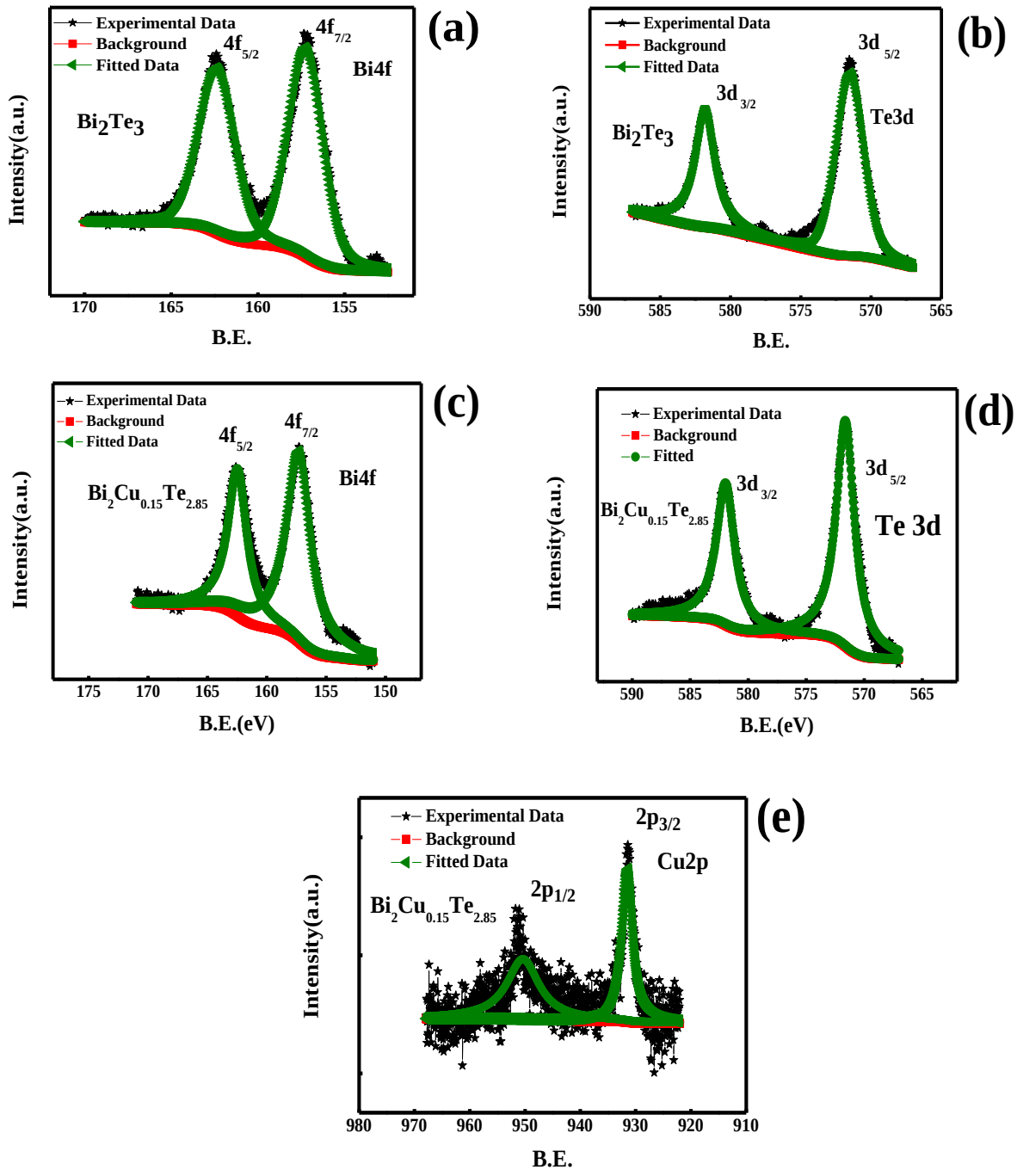

Fig.4.7 X-ray Photoemission core level spectrum of Bi and Te in Bi_2Te_3 sample (a) & (b) whereas (c), (d)&(e) show core level spectrum of Bi, Te and Cu in $Bi_2Cu_{0.15}Te_{2.85}$.

data observed in a Bi_2Te_3 single crystal [84]. Fig. 4.7(e) presents the high resolution XPS spectra of Cu2p levels in doped sample. Two peaks at 931.3 eV and 950.3 eV correspond to the $Cu2p^{3/2}$ and $Cu2p^{1/2}$ spin states respectively. Absence of strong or weak satellite peak

around 943eV rules out the presence of Cu^{2+} and Cu^{1+} state in the doped sample [85].Therefore, it is obvious that spin state of Cu is in Cu^0 state. Recently, it has been reported that defect may induce magnetic moment [86-89]. Gao et al. [86] reported that oxygen vacancy at the surface of ZnO nanoparticles are likely to be responsible for the ferromagnetism, Using first principle calculation Yazyev [87] found magnetism in graphene induced by single carbon atom defects whereas Hong et al. [88] observed room temperature ferromagnetism (RTFM) in different type of semiconducting and insulating oxide thin films such as HfO_2, TiO_2 and In_2O_3 due to the defects and oxygen vacancies. In another study, Maiti [89] found that, the exchange splitting in the impurity states having B2p character which originates due to the Boron vacancy, leads to a ferromagnetic state in CaB_6. The vacancy or defect phenomenon as discussed above might be a reason for the room temperature ferromagnetism (RTFM) in our Cu doped sample, as there is strong probability of site-antisite defects introduced by Cu which also causes tuning of carrier type from *n* to *p*. Further study is required to establish the exact origin and mechanism for defect introducing ferromagnetism in doped sample.

4.3 Conclusion

In this chapter we have investigated the structural, AIPES, magnetotransport and magnetic properties of Cu doped and undoped Bi_2Te_3 topological insulators. With Cu doping, resistivity increases as Fermi level is shifted into valence band with extra scattering centers. It is also observed that Cu doping tunes the carrier from *n* to *p* type, which is attributed to the presence of Te_{Bi} and Bi_{Te} antisites. The observed LMR is believed to be of classical origin and associated with gapless linear energy spectrum of surface Dirac Fermions along with disorderness in the sample. Moreover Cu doping induces room temperature ferromagnetism.

By developing such type of magnetic TIs a new way may open to design and develop future spintronics and electronic devices where high carrier concentration and mobility, large magnetoresistance and room temperature ferromagnetism (RTFM) is required.